Desalination 597 (2025) 118362

Contents lists available at ScienceDirect

Desalination

journal homepage: www.elsevier.com/locate/desal

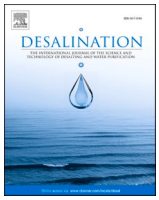

Can 3D-printed flow electrode gaskets replace CNC-milled graphite current collectors in flow capacitive deionization?

H.M. Saif [a], J.G. Crespo [a,b], S. Pawlowski [a,*]

[a] LAQV-REQUIMTE, DQ, FCT, Universidade NOVA de Lisboa, 2829-516 Caparica, Portugal
[b] Instituto de Tecnologia Química e Biológica António Xavier, Universidade NOVA de Lisboa, Av. da República, 2780-157 Oeiras, Portugal

HIGHLIGHTS

- 3D-printed gaskets can successfully replace CNC-milled graphite plates.
- Roughness of 3D-printed gaskets additionally enhances FCDI performance.
- 3D-printed conductive gaskets allow for 25 % higher FCDI desalination efficiency.
- The energy consumption was reduced by 10 % in FCDI cells with 3D-printed gaskets.
- 3D printing allows the fabrication of complex designs, impossible by CNC-milling.

GRAPHICAL ABSTRACT

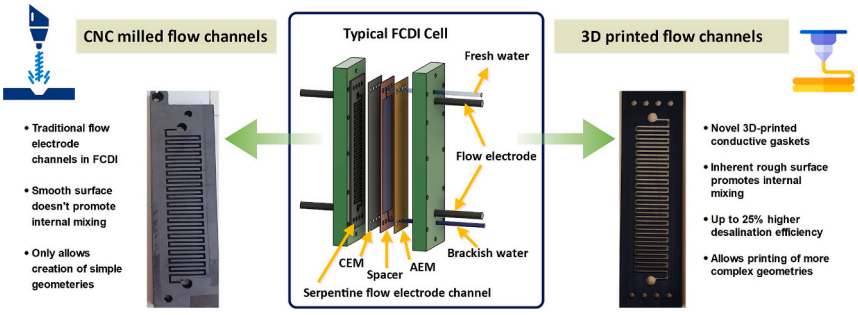

ARTICLE INFO

Keywords:
Desalination
Flow capacitive deionization (FCDI)
Current collectors
3D printing
CNC milling

ABSTRACT

As billions of people suffer from water scarcity, finding sustainable water resources is imperative. Flow capacitive deionization (FCDI) is a highly promising desalination process that can produce clean water from saline streams such as brackish and seawater. Conventional FCDI systems employ Computerised Numerical Control (CNC)-milled graphite plates that serve as current collectors and flow electrode channels. However, they have drawbacks such as high manufacturing costs, waste generation, and the difficulty of producing complex geometries required for efficient flow electrode mixing. Here, we successfully demonstrate that 3D-printed flow electrode gaskets, made of non-conductive polyethylene terephthalate glycol (PET-G) or a carbon black-infused conductive polylactic acid (PLA), are viable alternatives to traditional graphite plates. In specific cases, the desalination and energy efficiency in FCDI cells with 3D-printed conductive gaskets were even 25 % and 10 % higher, respectively, compared to traditional CNC-milled current collectors. The transition to 3D printing offers notable benefits, such as the competence to fabricate complex designs that enhance internal mixing and charge percolation. This innovation represents a change of paradigm in the way FCDI cells should be designed and manufactured, using additive manufacturing, which represents an efficient, scalable, and cost-effective substitute for the conventional approach, contributing therefore for the advancement of FCDI desalination technology.

* Corresponding author.
E-mail address: s.pawlowski@fct.unl.pt (S. Pawlowski).

https://doi.org/10.1016/j.desal.2024.118362
Received 2 September 2024; Received in revised form 1 November 2024; Accepted 25 November 2024
Available online 27 November 2024

1. Introduction

Around 4 billion people experience severe water scarcity for at least one month of the year, and half a billion face water shortage all over the year [1,2]. It is widely recognized that one of the most pressing challenges of the 21st century is the sustainable supply of fresh water [3,4]. In response to this challenge, emerging desalination technologies, such as flow capacitive deionization (FCDI), are gaining significant attention and have been actively studied over the past decade [5–10].

Contrary to capacitive deionization (CDI), where static porous carbon electrodes are employed, FCDI employs activated carbon slurries as flow electrodes instead of fixed porous carbon electrodes [11–13], while ion exchange membranes define ions transport from feed to receiver compartments [14]. The possibility to recirculate flow electrodes between anode and cathode allows for their continuous charging and discharging (regeneration), thus avoids their saturation and allows for continuous desalination in a single device, while the presence of ion exchange membranes increases the charge efficiency due to co-ions exclusion [15–17]. Besides being an energy-efficient, sustainable and environmentally friendly desalination process, FCDI has also been proposed for other applications, such as selective separation of different compounds like ammonia and fatty acids [18–20], removal of organic pollutants [21] and phosphorus [22], production of concentrated salt solutions [23], and extraction of valuable elements such as lithium and copper from saline streams [24,25].

Many efforts have been made to optimize the FCDI cell design to improve the desalination performance. Li et al. [26] employed different materials to build the feed compartment and a 54 % less energy consumption was observed when graphite plate was used compared to the polypropylene-made intermediate chamber. Ehring et al. [27] introduced a membrane-assisted static mixer in flow electrodes and reported a 250 % higher average salt removal rate compared to conventional flow electrode channel design. However, these static mixers are solely suitable for very low carbon mass loading in flow electrodes (<2 wt%). Likewise, Koller et al. [28] conducted a comparative analysis of various current collector architectures for FCDI applications. The bipolar current collector design was reported to be the most effective among the evaluated architectures, demonstrating a 55 % increase in salt removal compared to conventional graphite plate current collectors. However, the manufacturing process of bipolar current collectors is complex due to the need for advanced assembly techniques which limit their scalability. Saif et al. [29] demonstrated, through experimental and computational fluid dynamics (CFD) modelling insights, that the flow electrode channel design has a significant impact on FCDI performance, as the channel geometry strongly affects the local shear rate, and thus the local viscosity and flowability of flow electrodes, which are non-Newtonian fluids with shear-thinning behaviour. The prevalent configuration for flow electrode channels reported in the literature is the serpentine design, typically engraved in graphite plates by Computer Numerical Control (CNC) milling [5,11,15,30]. However, such serpentine design does not promote thorough mixing of the carbon particles [29], which is essential to facilitate charge percolation [31], and CNC milling has a limited capability to fabricate channels with more complex geometry which could enhance it [32]. Furthermore, CNC milling is a subtractive manufacturing technique, which creates waste and has limitations associated with material compatibility, lead times and customization [32,33]. Additionally, CNC milling is not a standard or easily accessible equipment. Alternatively, 3D printing is an additive manufacturing technique with several advantages over CNC milling, including customization freedom, the ability to create complex geometries, a wider selection of possible materials, waste reduction and rapid prototyping [34–36]. Furthermore, the expiration of protective patents made 3D printers cheap and widely available.

In this study, FCDI cells, with the conventional CNC-milled graphite plates and with 3D-printed flow electrode gaskets made of a) non-conductive polyethylene terephthalate glycol (PET-G) and b) a conductive mixture of polylactic acid (PLA) and carbon black (CB), were assembled and tested in terms of desalination efficiency, electrical properties and energy consumption. For a fair comparison between 3D printing and CNC milling, the same serpentine geometry was employed in all tests.

2. Experimental section

2.1. Design of 3D printing and CNC milling of flow electrode channels

The shape and dimensions of the tested flow electrode channels were identical for graphite plates and 3D-printed gaskets. The channel was a serpentine composed of 36 segments, each 2 mm thick, 2 mm deep and 34 mm long, as depicted in Fig. S1 in Supporting information. This is one of the most reported designs in the field of flow capacitive deionization [6,37–39]. The active contact area between the channel and the membrane was 26.58 cm^2. The computer-aided design (CAD) of such a serpentine channel was created using Autodesk Fusion 360 software.

2.1.1. 3D printing of non-conductive and conductive flow electrode gaskets

Flow electrode gaskets were manufactured using a ZMorph VX Multitool 3D Printer (Zmorph3D, Poland) by fused deposition modelling (FDM), which is based on the layer-by-layer extrusion of thermoplastic materials. The CAD with geometry was saved as a Standard Tessellation Language (.STL) file, which was translated into a geometric code (G-code) using Voxelizer 3.0 software. G-code is the set of instructions for the 3D printer to turn designs into physical objects. In 3D printing, one can control the material's filling inside the printed object depending on the final application of the object. Increasing internal filling leads to a mechanically more robust object, while a lower internal filling will lead to faster printing, but with poorer mechanical properties. Thus, the internal filling of gaskets was chosen to be 90 %, which led to the presence of some voids in the final structure.

The non-conductive gaskets were printed using a 1.75 mm Polyethylene Terephthalate Glycol (PET-G) filament from Dowire®, Portugal. The conductive gaskets were printed using a 1.75 mm filament, from Protopasta, USA, made of polylactic acid (PLA) and carbon black (CB). The materials which were employed are widely available, well-established and known for their stability. PET-G is resistant to water decomposition and exhibits good chemical stability and does not release harmful substances under normal conditions [40]. PLA is a biopolymer which biodegrades into lactic acid (LA) or to carbon dioxide and water. Moreover, it has been classified as Generally Recognized as Safe (GRAS) by the United States Food and Drug Administration (FDA) and has been found to be safe for all food packaging applications [41]. In this study, new gaskets were employed, but likewise prepared 3D-printed gaskets proved to be quite stable even after being used for nearly two years since no deterioration or alteration in their electrochemical performance was observed. To improve the first layer's adhesion with the 3D printer bed, a stick adhesive (AprintaPro PrintaStick) was used in both cases. Before printing the gaskets, the 3D printer was calibrated to ensure the best print quality. This involved testing the various FDM printing parameters, such as extrusion temperature, bed temperature, and printing speed. Fig. S2 in Supporting information shows the 3D-printed gaskets.

2.1.2. CNC milling of graphite plates

A ZMorph VX Multitool 3D Printer (Zmorph3D, Poland) was used to engrave flow electrode horizontal serpentine channels at the surface of graphite plates (25 cm length x 6 cm width x 1 cm thickness, Graphite Technologies, Portugal) by CNC milling. The CAD with geometry was exported as a drawing exchange (.DXF) file, which was transferred into Voxlizer 3.0 software to set the G-code with CNC milling parameters like milling bit size, speed and depth. The original and CNC-milled graphite plates can be seen in Fig. S3 in Supporting information.

2.2. Preparation of flow electrodes and feed solution

The YP50F activated carbon (Chemviron, Germany), specifically designed for electric double-layer capacitors, thus frequently used in FCDI, was employed to prepare the flow electrode slurry. Three different compositions, with 5, 10 and 15 wt% of YP50F were prepared in 1 g/L NaCl electrolyte. The upper concentration of 15 wt% of YP50F was chosen as at 20 wt% it was referred that the channels might clog [42]. These slurries were stirred for 24 h using a magnetic stirrer to attain a uniform carbon dispersion. The specific surface area of the activated carbon particles was determined by the Brunauer–Emmett–Teller (BET) method (ASAP2010, Micromeritics) and it was found to be 1600 m^2/g. The pore size distribution for YP50F activated carbon was also accessed using Barrett-Joyner-Halenda (BJH) method on the desorption branch of the isotherm and is presented in Fig. S4 in Supporting information. The highest pore volume was observed for micropores (1.7 nm) with some mesopores (2–50 nm) also having been observed. In the activated carbons, the coexistence of micropores and mesopores is important to achieve high salt removal efficiency in the FCDI process. Ion adsorption occurs at the electric double layer (EDL) formed at the internal surface of micropores while mesopores are crucial for effective ion transport to the adsorption sites. The combination of both micro and mesopores enables activated carbons to effectively store and release ions during the cyclic charging and discharging, which enables continuous desalination by FCDI [43]. The viscosity of carbon slurries was measured using a controlled stress rheometer (Thermo Scientific, HAAKE MARS III, Germany) equipped with a Peltier heating system and a coaxial cylinder geometry (Rotor CC25 DIN Ti). Viscosity values were recorded as a function of shear rate, in the range from 1 to 215 s^{-1}, at constant temperature (20 °C). 1.5 g/L NaCl aqueous solution was used as the feed solution in all experiments, because it mimics a typical salt concentration in brackish water.

2.3. Assembling of flow capacitive deionization (FCDI) cells

An electrodialysis stack (MEGA, Czech Republic) was used to create FCDI cells (with one feed compartment and two flow electrode compartments) [29,44]. Its platinum-coated titanium electrodes measuring 210 × 60 mm (length and width) were used as current collectors in FCDI cells with 3D-printed conductive and non-conductive gaskets that provided the path for the flow of carbon slurry. The assembly details of the FCDI cell with 3D-printed gaskets can be seen in Fig. S5 in Supporting information. In the case of FCDI cell with CNC-milled graphite plates, they were used instead of platinum-coated titanium electrodes and served as both a current collector and flow channels for the flow electrode. To stop water leaks and seal the flow electrode channels, a 12 mm × 0.075 mm MIARCO® polytetrafluoroethylene (PTFE) Teflon tape was used. Between the feed channel and the anode compartment, a Fumasep® FAB-PK-130 anion-exchange membrane was inserted, and a Fumasep® FKB-PK-130 cation-exchange membrane was installed between the feed channel and the cathode compartment. The thickness of each ion exchange membrane, both of which were provided by Fumatech GmbH, Germany, was 150 μm. The feed channel was 1.6 mm thick.

2.4. Desalination experiments

FCDI stacks with CNC-milled graphite plates, 3D-printed non-conductive gaskets and 3D-printed conductive gaskets were used in desalination experiments (Fig. 1). Model brackish water (1.5 g/L NaCl solution) was pumped in a single-passage mode through the feed channel at a flow rate of 2.5 mL/min using a peristaltic pump (Lead Fluid – BT100S, China). The flow electrode was recirculated through the FCDI cell in a closed loop at a flow rate of 100 mL/min using a peristaltic pump (Masterflex® L/S® Digital Peristaltic Pump Drive, UK). The total volume of flow electrode used in each experiment was 50 mL.

The cathodic and anodic flow electrodes were collected in a continuously stirred reservoir to assure the mixing and neutralization of oppositely charged flow electrodes and, therefore, to release the ions electrostatically adsorbed during desalination on the surface of activated carbon particles [45]. Each desalination experiment was performed for 1 h, during which a constant voltage of 1.2 V was applied using a Vertex 5A potentiostat (Ivium Technologies, The Netherlands). The conductivity of the effluent was measured at the exit of the FCDI cell every 2 s using a conductivity meter (Horiba Laqua-PC1100, Japan). The associated error with the conductivity measurement device was ±0.5 %. The conductivity values were converted into NaCl concentration using

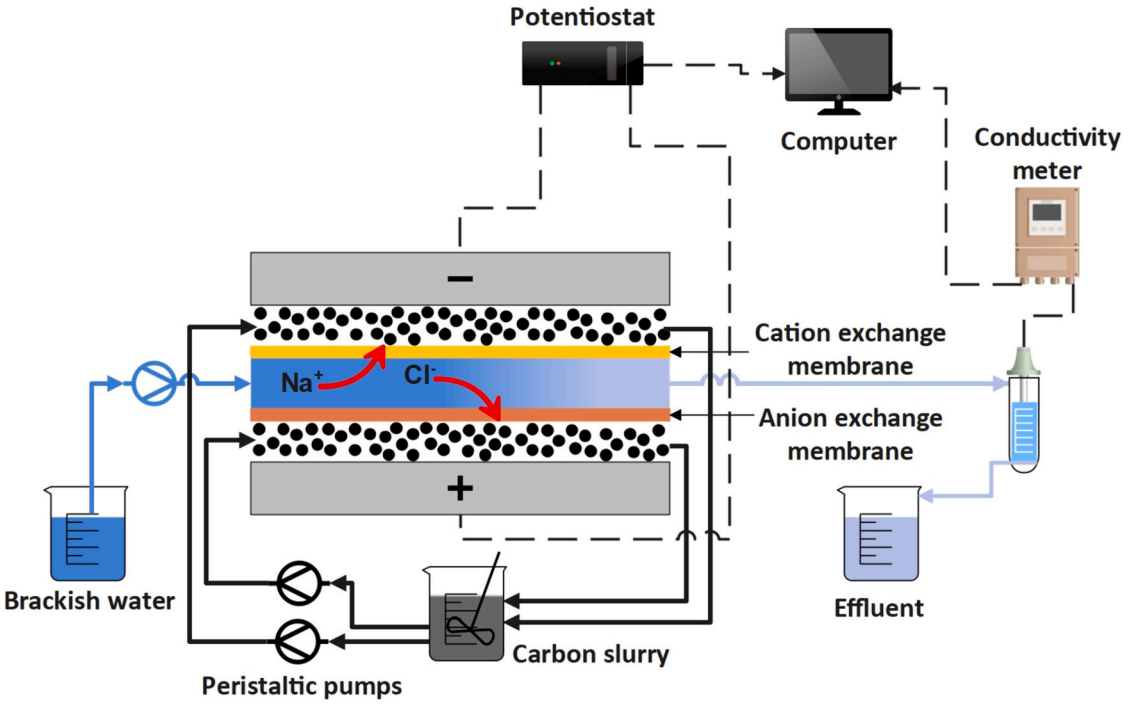

Fig. 1. Schematic illustration of the flow-electrode capacitive deionization (FCDI) system used in this study.

the calibration curve (Fig. S6) reported in Supporting information.

The desalination efficiency was calculated as follows [46,47]:

$$\textit{Desalination efficiency}\ (\%) = \frac{C_f - C_e}{C_f} \times 100 \quad (1)$$

where C_f is the initial NaCl concentration and C_e is the effluent NaCl concentration (mM).

Energy (E) required to remove 1 mol of NaCl (W.h/mol$_{NaCl}$) was calculated as follows:

$$\Gamma = \int_0^t Q(C_f - C_e)dt \quad (2)$$

$$E = \frac{V \int_0^t I\,dt}{t \cdot \Gamma} \quad (3)$$

where Γ is the accumulated salt removal (mol), Q is the volumetric flow rate of feed (m^3/s), V is the applied potential difference (V), I is the electrical current (A) passing through the FCDI cell during the desalination experiment, and t is the time (s) of the desalination experiment.

2.5. Roughness measurements

The micro roughness of 3D-printed gaskets and CNC-milled graphite plates was measured using a KLA Tencor Alpha Step 200 Profilometer, USA. For each measurement, a 2000 μm length of each material was scanned at a scan rate of 50 μm/s. Two readings were taken for each measurement and average roughness was reported.

2.6. X-ray tomography

The samples were scanned using nano-CT (SkyScan 2214, Bruker, Belgium). An X-ray tube using a tungsten (W) source (operated at 50 kV and 110 μA) without a filter was used to acquire the images. A voxel size of 2.5 μm was selected. During data acquisition, the capillaries were rotated 360° and the images were taken every 0.4°. An exposure time of 2000 ms was used for non-conductive (PET-G) after use, and conductive (PLA + carbon) after use; 2100 ms for conductive (PLA + carbon) before use; and 2200 ms for non-conductive (PET-G) before use. A frame averaging of 3 was employed. No binning was employed. The flat panel was selected as the detector system. The reconstruction of the CT was done using the NRecon software (version 2.2.0.6, Bruker) based on the Feldkamp algorithm. CTAn software (version 1.20.8.0, Bruker) was used for the 3D analysis. A region of interest (ROI) representative of the sample was selected and, the images were binarized. The quantitative analyses of the sample were then performed through the 3D plug-in analysis. CTVox software (Bruker) (version 3.3.1, Bruker) was used for volume rendering.

2.7. Electrochemical properties

The electrical conductance of the 3D-printed gaskets and CNC-milled graphite plate was evaluated before and after desalination experiments by linear sweep voltammetry (LSV) performed using a Vertex 5A potentiostat (Ivium Technologies). A scan rate of 0.5 mV/s, at a step of 1 mV for the potential difference range between −0.5 V and +0.5 V was used to obtain current-voltage curves whose slope is the conductance of the material under analysis [48]. The electrical resistivity of the tested materials was calculated as follows:

$$\rho = \frac{1}{\kappa} \times \frac{A}{L} \quad (4)$$

where ρ (Ω·m) is electrical resistivity, κ (S) is the electrical conductance, L (m) is the length and A (m^2) is the cross-section area of the tested material.

Electrochemical impedance spectroscopy (EIS) was also performed to measure the capacitance of flow electrodes at the end of each experiment. The feed solution (1.5 g/L NaCl) was pumped through the FCDI cell until the effluent conductivity values became equal to the feed conductivity. This step was done to maintain the feed channel resistance constant to avoid its influence on the capacitance measurements of the flow electrodes. EIS was performed on the same FCDI setup that was used in desalination tests in a frequency range of 10 kHz to 10 mHz with a sine wave signal amplitude of 10 mV using a Vertex 5A potentiostat (Ivium Technologies, The Netherlands). The capacitance was calculated by the following equation [46].

$$C = \left| \frac{1}{\omega Z''} \right| \quad (5)$$

where C (F) is the capacitance, ω (Hz) is the angular frequency of the applied alternating current (AC) signals and Z'' (Ω) is the imaginary resistance of the impedance.

3. Results and discussion

3.1. Desalination performance

To analyse the desalination performance of FCDI cells with CNC-milled graphite plates and 3D-printed non-conductive and conductive gaskets, desalination experiments were performed using 1.5 g/L of NaCl aqueous feed solution. The electric current at FCDI cells was recorded during experiments and is shown in Fig. 2.

In the case of 3D-printed non-conductive and conductive gaskets, there was a gradual increase in current values for all the composition of flow electrodes (5, 10 and 15 wt%), which indicates a progressive increase of the salt amount being removed from the feed. This effect can be confirmed when looking at the conductivity of the effluent (Fig. 3), which continuously decreased over time in FCDI cells with 3D-printed non-conductive and conductive gaskets. The initial and final NaCl concentration in the effluent for each desalination experiment can be seen in Table S1 in Supporting information.

Both observations indicate that the FCDI performance increased over time when using 3D-printed flow electrode channel gaskets. On the other hand, when traditional CNC-milled graphite flow electrode channels were used, the amount of current passing through the FCDI cell was constant over time (when using 15 wt% flow electrodes) or slightly decreased (when using 5 and 10 wt% flow electrodes). This translated into a constant effluent concentration in the FCDI cell with CNC-milled graphite plates when using 15 wt% flow electrode and an increase of effluent concentration when using flow electrodes with 5 wt% and 10 wt % of YP50F. To better understand the FCDI desalination performance, the desalination efficiency (at $t = 1$ h) and specific energy consumption during 1 h of operation were calculated (Fig. 4).

When 5 and 10 wt% YP50F carbon slurries were used as flow electrodes, the FCDI cells with 3D-printed gaskets outperformed the FCDI cell with CNC-milled graphite plates in terms of desalination efficiency. When 15 wt% flow electrodes were used, the highest desalination efficiency was obtained in FCDI cell with CNC-milled graphite plates followed by FCDI cells with 3D-printed conductive and non-conductive gaskets. The energy consumption has the reverse trends of desalination efficiency.

3.2. Resistivity and surface roughness of flow electrode gaskets

To understand the different behaviour of FCDI cells when using 5 and 10 wt% flow electrodes compared to 15 wt% flow electrodes, the resistivity of the employed materials (Fig. 5) and their surface roughness (Fig. 6) were analysed.

For FCDI cells with 15 wt% flow electrodes, the desalination trends follow the resistivity of the materials which is the lowest for CNC-milled graphite plates (2.78×10^{-4} Ω.m), followed by 3D-printed conductive

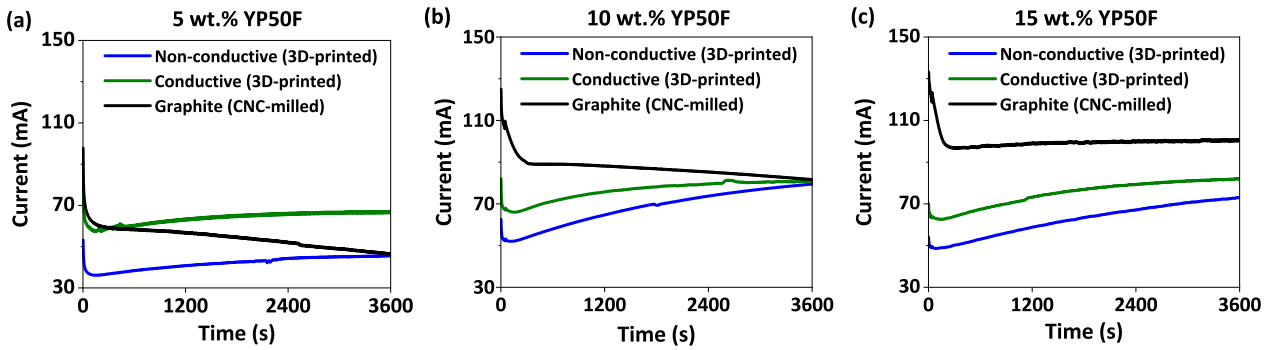

Fig. 2. Chronoamperometric curves obtained at FCDI stacks with 3D-printed (non-conductive and conductive) and CNC-milled (graphite) flow electrode channels when using flow electrodes with (a) 5 wt%, (b) 10 wt% and (c) 15 wt% of YP50F during desalination of aqueous solution with 1.5 g/L of NaCl.

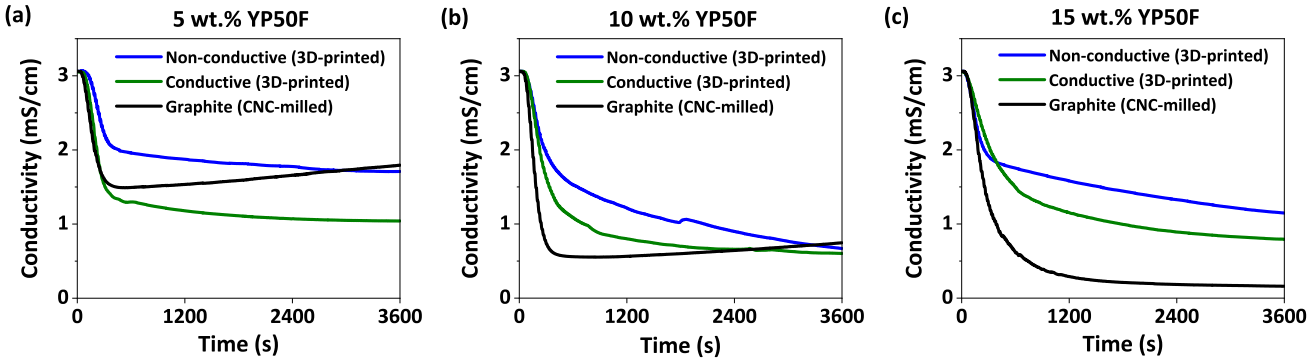

Fig. 3. Effluent conductivity at FCDI stacks with 3D-printed (non-conductive and conductive) and CNC-milled (graphite) flow electrode channels when using flow electrodes with (a) 5 wt%, (b) 10 wt% and (c) 15 wt% of YP50F during desalination of aqueous solution with 1.5 g/L of NaCl.

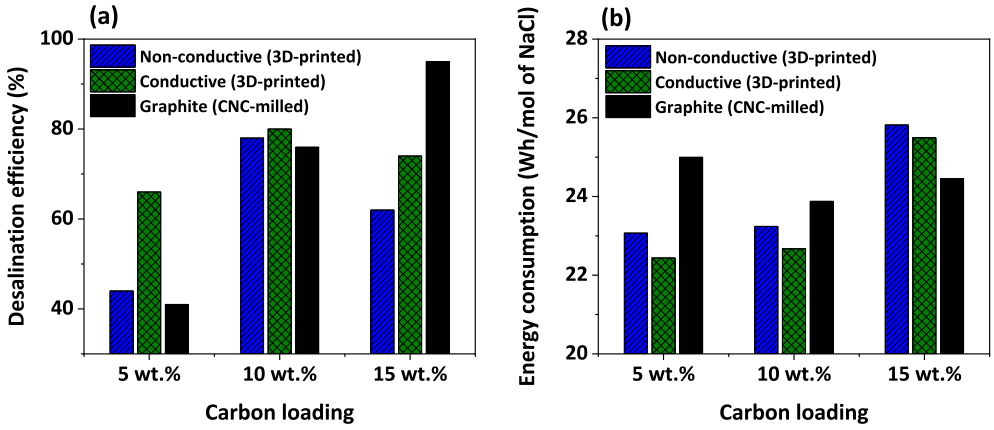

Fig. 4. (a) Desalination efficiency (%) and (b) energy consumption (W.h/mol of NaCl) of FCDI stacks with different 3D-printed (non-conductive and conductive) and CNC-milled (graphite) flow electrode channels when using flow electrodes with 5, 10 and 15 wt% of YP50F during desalination of aqueous solution with 1.5 g/L of NaCl.

(0.88 Ω.m) and non-conductive (4.16×10^7 Ω.m) gaskets. Since graphite plate resistivity is the lowest one, it would be expected that the desalination efficiency will be the highest (something which was only observed when using 15 wt% flow electrodes). What is also interesting to observe is that the resistivity values are not constant (at least for the 3D-printed materials); pristine 3D-printed gaskets had higher resistivity than the used ones. This decrease of the resistivity, by 28 % and 17 % for conductive and non-conductive gaskets, respectively, after being used for 1 h, explains why the current was increasing over time in FCDI cells with 3D-printed gaskets, and why it was constant when using graphite plates (which resistivity kept constant). The decrease in the resistivity of 3D-printed materials was caused by the penetration of highly capacitive YP50F activated carbon particles (164 F/g) [49] into the void spaces of 3D-printed structures. The 3D-printed non-conductive gasket before and after use are shown in Fig. S6 in Supporting information. After use in the desalination tests, the black colour of the gasket evidences the presence of highly capacitive YP50F carbon particles retained inside the voids of the 3D-printed gasket. This was confirmed by X-ray tomography (Fig. 7 and Videos 1–4), of which the comprehensive analysis is presented in Section 3.3.

However, as previously mentioned, for 5 and 10 wt% flow electrodes the desalination efficiency was the highest in the FCDI cell with

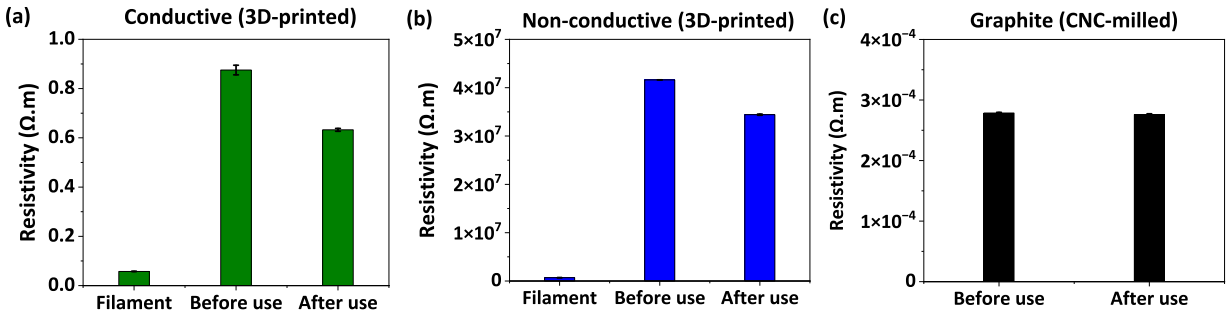

Fig. 5. The resistivity of 3D-printed (a) conductive, (b) non-conductive and (c) CNC-milled graphite flow electrode channels gaskets before and after use in the FCDI experiment.

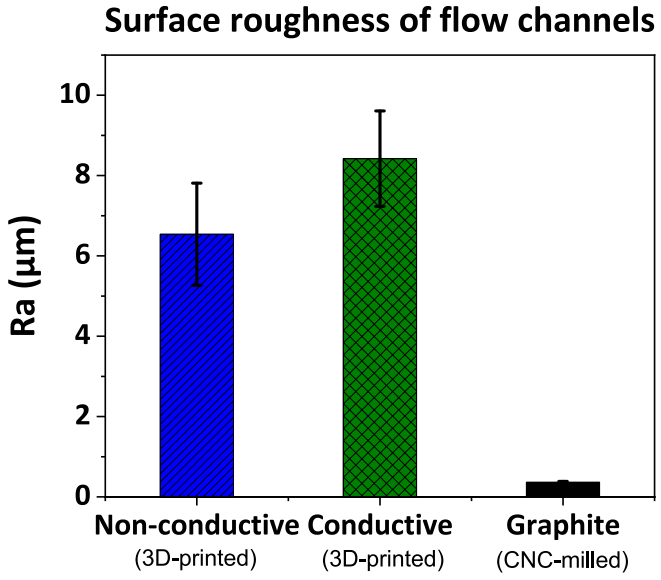

Fig. 6. Surface roughness of 3D-printed non-conductive, conductive gaskets and CNC-milled graphite plate.

conductive gaskets, followed by the FCDI cell with non-conductive gaskets and finally the one with the graphite plates. When the concentration of carbon particles in a slurry decreases, the viscosity of the fluid decreases (Supporting information Fig. S8) which facilitates the internal mixing of flow electrodes. The viscosity of flow electrodes decreases if the local shear rate increases [29], which can be achieved by the introduction of corrugations on the surface of the channel. Corrugations in the flow channels promote the localized mixing and interaction between the flow electrodes and channel walls by generating micro-scale vortices that improve charge transfer efficiency. This effect, especially in laminar flow, disrupts boundary layers, facilitating ion exchange and improving flow-electrode performance [50]. In the case of 3D-printed materials, their surface is not perfectly smooth due to the method of their manufacturing, which is the deposition of thin melted lines of materials, layer-by-layer, which can be seen and felt with the naked eye. When analysing the roughness of the employed materials (Fig. 6), indeed the highest one was measured for the conductive gasket, followed closely by non-conductive gaskets, and almost without any rugosity in the case of graphite plates. Thus, when using flow electrodes with lower carbon content (5 and 10 wt%), which are already more prone for mixing, the roughness of the 3D-printed gaskets further promotes their mixing compared with graphite plates, which explains the higher desalination efficiency.

3.3. X-ray tomography of flow electrode gaskets

To visualize the incorporation of carbon particles and the surface roughness of the 3D-printed gaskets, X-ray tomography of specific sections of the 3D-printed gaskets was performed.

In Fig. 7 it is possible to visualize that the gaskets are made of cylindrical sections, deposited layer-by-layer during 3D printing, which leads to the roughness of the gasket surfaces, thus the gaskets' surface is not smooth. It is also possible to observe the existence of empty spaces between those 3D-printed layers, and their occupation by carbon particles after being used. The Supporting information contains detailed videos that illustrate these observations. Additionally, image analysis of the obtained virtual reconstructions allowed to estimate parameters such as material porosity or the size of the carbon particles. The selected pristine segments of the non-conductive and conductive gaskets have a porosity of 8 and 6.5 %, respectively. The intended infill chosen during 3D printing was 90 %, thus the values are close to expected. After use, 0.7 % of the empty spaces in the tested conductive segment were filled by activated carbon particles with an average particle size of 9.6 µm. In the case of the tested non-conductive gasket, the values were 0.6 % and 10.8 µm. The average size of YP50F carbon particles measured by the particle size analyzer (Laser Scattering Particle Size Distribution Analyzer LA-960, HORIBA, Japan) is 9.33 µm (Fig. S9 in Supporting information shows the YP50F particle size distribution), which is in accordance with the particle size detected by tomography. Furthermore, since more voids were filled with smaller carbon particles in the conductive gaskets, it explains the higher decrease in resistivity values for conductive gaskets (27 %) compared to the non-conductive ones (17 %).

3.4. Capacitance of flow electrodes

The desalination performance was also validated by assessing the capacitance of the flow electrodes at the end of the FCDI experiments with 3D-printed gaskets and CNC-milled graphite current collectors (Fig. 8).

As seen in Fig. 8, flow electrodes have no capacitance in the high frequency region but there are significant differences in their values at the low frequency range (below 10 mHz). At high frequencies, ions came closer to the pores of activated carbon particles in the flow electrode, while at low frequencies ions propagate deep inside the pores. Hence, the capacitive behaviour of the flow electrode can only be observed at low frequencies [46,51,52]. For 5 and 10 wt% flow electrodes, the highest capacitance was observed when using 3D-printed conductive gaskets, then non-conductive ones and the least for CNC-milled graphite plates. The observed high capacitance when using 3D-printed conductive gaskets as flow electrode channels could be explained by their high surface roughness which enhances the mixing of flow electrodes, thus leading to more effective charge percolation between carbon particles.

In contrast, for 15 wt% flow electrodes, the highest desalination efficiency and capacitance were obtained when CNC-milled graphite flow

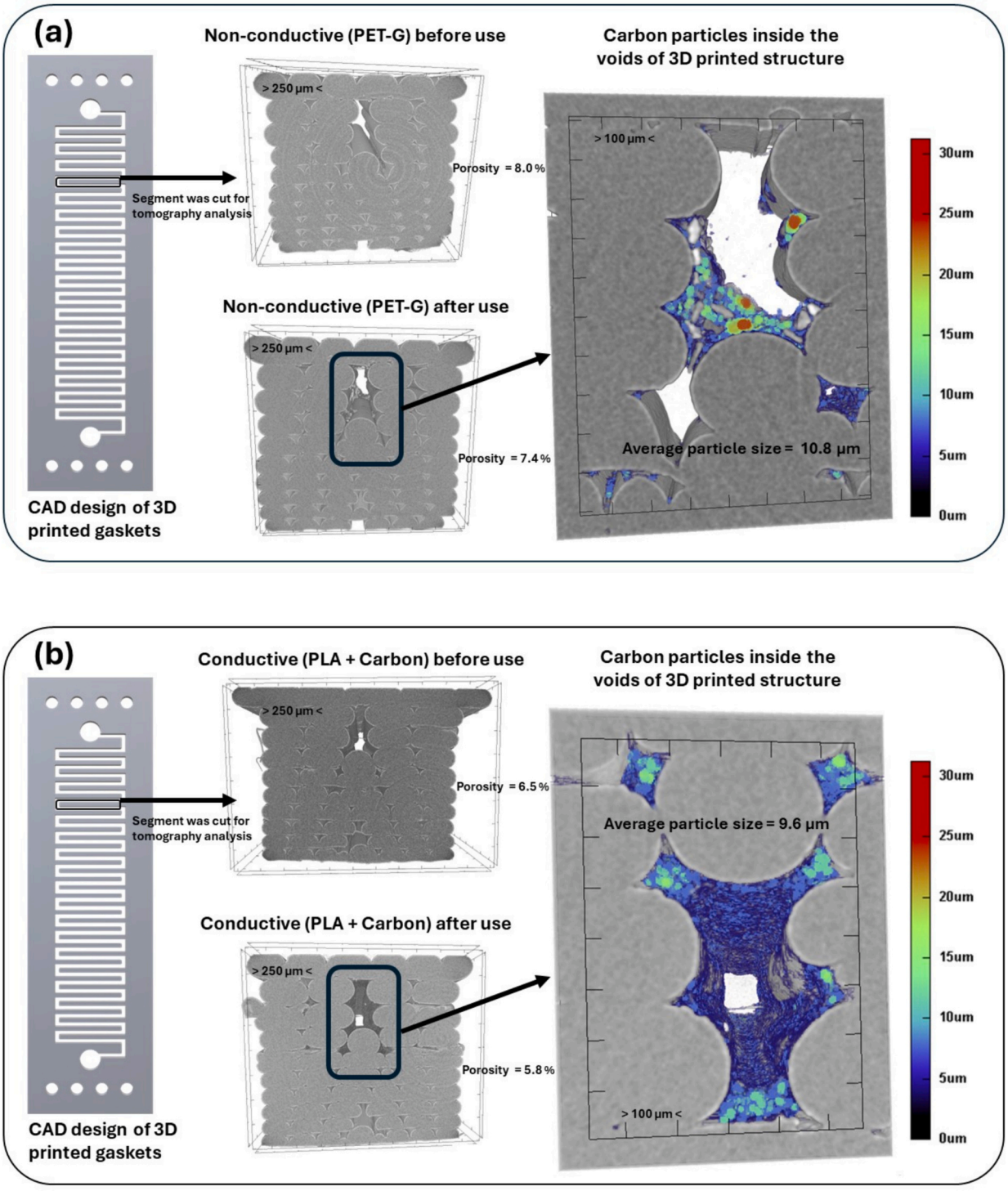

Fig. 7. X-ray tomography of (a) 3D-printed non-conductive (PET-G) and (b) 3D-printed conductive (PLA + carbon) gaskets.

electrode channels were used. This could be explained by higher viscosity and concentration of carbon particles in the flow electrode. The viscosity of the flow electrode increases with an increase in the weight percentage of carbon. At a 15 wt% of carbon loading in the flow electrode, the viscosity is about 10 and 3 times higher compared to 5 wt% and 10 wt% of carbon loading, respectively, which hinders mixing of the flow electrode and results in a poor charge transfer even in the 3D-printed rough flow electrode channels. Thus, for flow electrodes with 15 wt% of carbon loading, the dominant parameter is the resistance of flow electrode channels, as the resistance of pristine graphite plates is minimal compared to 3D-printed conductive and non-conductive gaskets (Fig. 5).

4. Conclusions

This study addresses the need to develop an alternative to CNC-milled graphite current collectors, which are difficult to manufacture and offer limited flow channel design options. The findings presented in this study indicate that the use of 3D printing technology can replace traditional CNC-milled graphite plates. Either non-conductive or

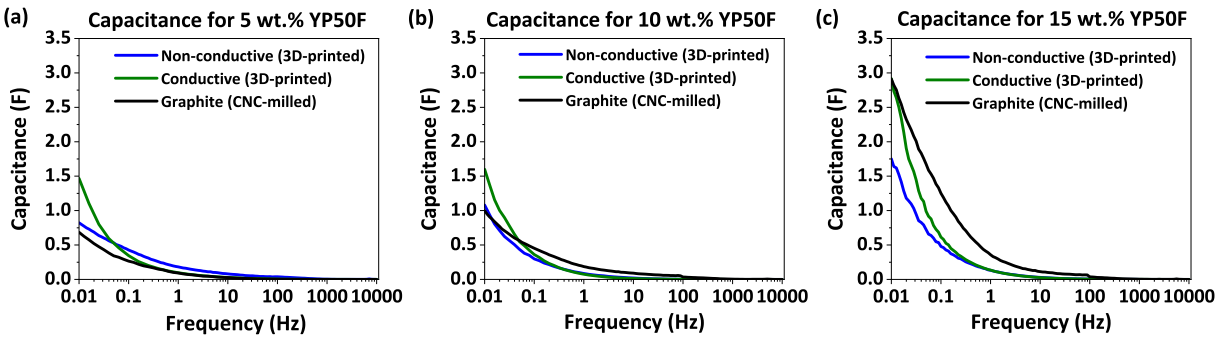

Fig. 8. The capacitance of the (a) 5 wt% (b) 10 wt% and (c) 15 wt% YP50F flow electrodes measured at the end of the experiment as a function of frequency.

conductive 3D printed gaskets have promising potential, but the conductive ones offer more advantages, besides their rough surface that facilitates internal mixing and charge percolation, because they exhibit a lower electrical resistance when compared with non-conductive gaskets. Although further studies are still needed to explore the best flow electrode channel design for efficient mixing and salt removal in the FCDI process, 3D printing opens a very promising perspective to proceed with necessary modifications in the design of flow channels, enhancing the local shear rate. This is especially crucial for shear-thinning fluids, such as activated carbon slurries, where the local shear rate substantially impacts the viscosity and, as a result, the overall efficiency of the mixing process.

Supplementary data to this article can be found online at https://doi.org/10.1016/j.desal.2024.118362.

CRediT authorship contribution statement

Hafiz M. Saif: Conceptualization, Methodology, Validation, Investigation, Data Curation, Writing - Original Draft, Visualization; **João G. Crespo**: Conceptualization, Writing - Review & Editing, Supervision, Project administration, Funding acquisition; **Sylwin Pawlowski**: Conceptualization, Methodology, Resources, Data Curation, Writing - Review & Editing, Supervision, Project administration, Funding acquisition.

Declaration of competing interest

The authors declare that they have no known competing financial interests or personal relationships that could have appeared to influence the work reported in this paper.

Acknowledgements

This work received funding from Fundação para a Ciência e a Tecnologia, I.P. (FCDT/MCTES) under grant agreement No PTDC/EQU-EQU/6193/2020 (Se(L)ect(i)vity). This work received funding from the European Union Horizon 2020 research and innovation programme under grant agreement No 869467 (SEArcularMINE). This work was also supported by the Associate Laboratory for Green Chemistry – LAQV which is financed by national Portuguese funds from FCT/MCTES (UIDB/50006/2020). Hafiz Muhammad Saif Ullah Saleem acknowledges FCT/MCTES for his PhD grant 2020.09828.BD (doi:10.54499/2020.09828.BD). The authors acknowledge Professor Vítor D. Alves, from Instituto Superior de Agronomia, Universidade de Lisboa, for providing support in the analysis of the rheology of the carbon slurries.

Data availability

Data will be made available on request.

References

[1] C. Zhang, D. He, J. Ma, W. Tang, T.D. Waite, Faradaic reactions in capacitive deionization (CDI) - problems and possibilities: a review, Water Res. 128 (2018) 314–330, https://doi.org/10.1016/j.watres.2017.10.024.
[2] M.M. Mekonnen, A.Y. Hoekstra, Four billion people facing severe water scarcity, Sci. Adv. 2 (2016) 1–6, https://doi.org/10.1126/sciadv.1500323.
[3] S. Xu, A.J. Hutchinson, M. Taheri, B. Corry, J.F. Torres, Thermodiffusive desalination, Nat. Commun. 15 (2024), https://doi.org/10.1038/s41467-024-47313-5.
[4] M. Elimelech, W.A. Phillip, The future of seawater desalination: energy, technology, and the environment, Science 333 (2011) (1979) 712–717, https://doi.org/10.1126/science.1200488.
[5] C. Zhang, J. Ma, L. Wu, J. Sun, L. Wang, T. Li, T.D. Waite, Flow electrode capacitive deionization (FCDI): recent developments, environmental applications, and future perspectives, Environ. Sci. Technol. 55 (2021) 4243–4267, https://doi.org/10.1021/acs.est.0c06552.
[6] K. Luo, T. Hu, W. Xing, G. Zeng, W. Tang, Polyaniline/activated carbon composite based flowing electrodes for highly efficient water desalination with single-cycle operational mode, Chem. Eng. J. 481 (2024), https://doi.org/10.1016/j.cej.2023.148454.
[7] A. Carmona-Orbezo, R.A.W. Dryfe, Understanding the performance of flow-electrodes for capacitive deionization through hydrodynamic voltammetry, Chem. Eng. J. 406 (2021), https://doi.org/10.1016/j.cej.2020.126826.
[8] R. Chen, X. Liu, M. Wang, Y. Shu, M. Zhang, B. Liu, Z. Wang, A novel two-stage continuous capacitive deionization system with connected flow electrode and freestanding electrode, Chem. Eng. J. 491 (2024), https://doi.org/10.1016/j.cej.2024.152133.
[9] L. Yan, S. Issaka Alhassan, H. Gang, B. Wu, D. Wei, Y. Cao, P. Chen, H. Wang, Enhancing charge transfer utilizing ternary composite slurry for high-efficient flow-electrode capacitive deionization, Chem. Eng. J. 468 (2023), https://doi.org/10.1016/j.cej.2023.143413.
[10] H.J. Chung, J. Kim, D.I. Kim, G. Gwak, S. Hong, Feasibility study of reverse osmosis–flow capacitive deionization (RO-FCDI) for energy-efficient desalination using seawater as the flow-electrode aqueous electrolyte, Desalination 479 (2020), https://doi.org/10.1016/j.desal.2020.114326.
[11] S. Il Jeon, H.R. Park, J.G. Yeo, S. Yang, C.H. Cho, M.H. Han, D.K. Kim, Desalination via a new membrane capacitive deionization process utilizing flow-electrodes, energy, Environ. Sci. 6 (2013) 1471–1475, https://doi.org/10.1039/c3ee24443a.
[12] J. Nordstrand, SofTer: theory, software, and video tutorial for simulating capacitive deionization with tertiary current distributions, Desalination 566 (2023), https://doi.org/10.1016/j.desal.2023.116899.
[13] J.G. Gamaethiralalage, K. Singh, S. Sahin, J. Yoon, M. Elimelech, M.E. Suss, P. Liang, P.M. Biesheuvel, R.L. Zornitta, L.C.P.M. De Smet, Recent advances in ion selectivity with capacitive deionization, energy, Environ. Sci. 14 (2021) 1095–1120, https://doi.org/10.1039/d0ee03145c.
[14] K. Dehghan, S.A. Mirbagheri, M. Alam, Investigation of effective parameters on brackish water desalination by flow-electrode capacitive deionization, Water Supply 22 (2022) 5176–5189, https://doi.org/10.2166/ws.2022.153.
[15] F. Yu, Z. Yang, Y. Cheng, S. Xing, Y. Wang, J. Ma, A comprehensive review on flow-electrode capacitive deionization: design, active material and environmental application, Sep. Purif. Technol. 281 (2022), https://doi.org/10.1016/j.seppur.2021.119870.
[16] Y.U. Shin, J. Lim, C. Boo, S. Hong, Improving the feasibility and applicability of flow-electrode capacitive deionization (FCDI): review of process optimization and energy efficiency, Desalination 502 (2021), https://doi.org/10.1016/j.desal.2021.114930.
[17] S. Yang, S. Il Jeon, H. Kim, J. Choi, J.G. Yeo, H.R. Park, D.K. Kim, Stack design and operation for scaling up the capacity of flow-electrode capacitive deionization technology, ACS Sustain. Chem. Eng. 4 (2016) 4174–4180, https://doi.org/10.1021/acssuschemeng.6b00689.
[18] P. Nativ, O. Lahav, Y. Gendel, Separation of divalent and monovalent ions using flow-electrode capacitive deionization with nanofiltration membranes, Desalination 425 (2018) 123–129, https://doi.org/10.1016/j.desal.2017.10.026.

[19] K. Fang, H. Gong, W. He, F. Peng, C. He, K. Wang, Recovering ammonia from municipal wastewater by flow-electrode capacitive deionization, Chem. Eng. J. 348 (2018) 301–309, https://doi.org/10.1016/j.cej.2018.04.128.
[20] G.Y. Wu, Y. Pu, Y. Wang, H. Zhang, Q. Wu, R.J. Zeng, Y. Jiang, Selective recovery of medium-chain fatty acids from secondary fermentation broth by flow-electrode capacitive deionization, Chem. Eng. J. 470 (2023), https://doi.org/10.1016/j.cej.2023.144168.
[21] X. Wang, F. Qi, S. Wang, P. Zhu, X. Wei, Z. Li, J. Zhao, Simultaneous desalination and removal of organic pollutants in a novel bifunctional FCDI system: the enhancement by in-situ reutilization of chloride ions, Desalination 592 (2024), https://doi.org/10.1016/j.desal.2024.118107.
[22] Y. He, X. Zhang, K. Zuo, F. Yang, T. Gao, P. Liang, Highly efficient and selective extraction of phosphorous from wastewater as vivianite in a strategically operated four-chamber flow electrode capacitive deionization, Desalination 544 (2022), https://doi.org/10.1016/j.desal.2022.116089.
[23] C.J. Linnartz, A. Rommerskirchen, M. Wessling, Y. Gendel, Flow-electrode capacitive deionization for double displacement reactions, ACS Sustain Chem Eng 5 (2017) 3906–3912, https://doi.org/10.1021/acssuschemeng.6b03086.
[24] H.M. Saif, J.G. Crespo, S. Pawlowski, Lithium recovery from brines by lithium membrane flow capacitive deionization (Li-MFCDI) – a proof of concept, Journal of Membrane Science Letters 3 (2023) 100059, https://doi.org/10.1016/j.memlet.2023.100059.
[25] X. Zhang, F. Yang, J. Ma, P. Liang, Effective removal and selective capture of copper from salty solution in flow electrode capacitive deionization, Environ Sci (Camb) 6 (2020) 341–350, https://doi.org/10.1039/c9ew00467j.
[26] Y. Li, C. Yang, M. Chen, Y. Bian, J. Niu, S. Mu, J. Zhang, C. Liu, J. Ma, Optimization of the intermediate chamber improves desalination performance in flow electrode capacitive deionization (FCDI): a comparative study, Desalination 584 (2024), https://doi.org/10.1016/j.desal.2024.117743.
[27] J.C. Ehring, A.V. Mizrak, L. Agartan, B. Aküzüm, E.C. Kumbur, A new static mixer concept for enhanced desalination performance in flow-electrode capacitive deionization (FCDI) systems, Desalination 566 (2023), https://doi.org/10.1016/j.desal.2023.116887.
[28] N. Köller, M. Perrey, L.K. Brückner, P. Schäfer, S. Werner, C.J. Linnartz, M. Wessling, Comparison of current collector architectures for flow-electrode capacitive deionization, Desalination 582 (2024), https://doi.org/10.1016/j.desal.2024.117595.
[29] H.M. Saif, T.H. Gebregeorgis, J.G. Crespo, S. Pawlowski, The influence of flow electrode channel design on flow capacitive deionization performance: experimental and CFD modelling insights, Desalination 578 (2024) 117452, https://doi.org/10.1016/j.desal.2024.117452.
[30] K. Fang, H. Gong, W. He, F. Peng, K. Wang, Revealing the intrinsic differences between static and flow electrode capacitive deionization by introducing semi-flow electrodes, Environ Sci (Camb) 6 (2020) 362–372, https://doi.org/10.1039/c9ew00836e.
[31] F. Yang, Y. He, L. Rosentsvit, M.E. Suss, X. Zhang, T. Gao, P. Liang, Flow-electrode capacitive deionization: a review and new perspectives, Water Res. 200 (2021), https://doi.org/10.1016/j.watres.2021.117222.
[32] H.T. Yau, T.J. Yang, Y.K. Lin, Comparison of 3-D printing and 5-axis milling for the production of dental e-models from intra-oral scanning, Comput Aided Des Appl 13 (2016) 32–38, https://doi.org/10.1080/16864360.2015.1059186.
[33] T. Pereira, J.V. Kennedy, J. Potgieter, A Comparison of Traditional Manufacturing Vs Additive Manufacturing, the Best Method for the Job, Procedia Manuf, Elsevier B.V, in, 2019, pp. 11–18, https://doi.org/10.1016/j.promfg.2019.02.003.
[34] D. Fico, D. Rizzo, F. Montagna, C. Esposito Corcione, Fused filament fabrication and computer numerical control milling in cultural heritage conservation, Materials 16 (2023), https://doi.org/10.3390/ma16083038.
[35] W. Gao, Y. Zhang, D. Ramanujan, K. Ramani, Y. Chen, C.B. Williams, C.C.L. Wang, Y.C. Shin, S. Zhang, P.D. Zavattieri, The status, challenges, and future of additive manufacturing in engineering, CAD Computer Aided Design 69 (2015) 65–89, https://doi.org/10.1016/j.cad.2015.04.001.
[36] C. Esposito Corcione, F. Gervaso, F. Scalera, S.K. Padmanabhan, M. Madaghiele, F. Montagna, A. Sannino, A. Licciulli, A. Maffezzoli, Highly loaded hydroxyapatite microsphere/PLA porous scaffolds obtained by fused deposition modelling, Ceram. Int. 45 (2019) 2803–2810, https://doi.org/10.1016/j.ceramint.2018.07.297.
[37] J. Lim, H. Lee, S. Lee, S. Hong, Capacitive deionization incorporating a fluidic MOF-CNT electrode for the high selective extraction of lithium, Desalination 578 (2024), https://doi.org/10.1016/j.desal.2024.117403.
[38] F. Yang, J. Ma, X. Zhang, X. Huang, P. Liang, Decreased charge transport distance by titanium mesh-membrane assembly for flow-electrode capacitive deionization with high desalination performance, Water Res. 164 (2019), https://doi.org/10.1016/j.watres.2019.114904.
[39] Y. Gendel, A.K.E. Rommerskirchen, O. David, M. Wessling, Batch mode and continuous desalination of water using flowing carbon deionization (FCDI) technology, Electrochem. Commun. 46 (2014) 152–156, https://doi.org/10.1016/j.elecom.2014.06.004.
[40] Harry, Is PETG Safe? Unveiling the Facts, (n.d.). https://www.immould.com/is-petg-safe/ (accessed October 21, 2024).
[41] T.A. Swetha, A. Bora, K. Mohanrasu, P. Balaji, R. Raja, K. Ponnuchamy, G. Muthusamy, A. Arun, A comprehensive review on polylactic acid (PLA) – synthesis, processing and application in food packaging, Int. J. Biol. Macromol. 234 (2023), https://doi.org/10.1016/j.ijbiomac.2023.123715.
[42] S. Porada, D. Weingarth, H.V.M. Hamelers, M. Bryjak, V. Presser, P.M. Biesheuvel, Carbon flow electrodes for continuous operation of capacitive deionization and capacitive mixing energy generation, J Mater Chem A Mater 2 (2014) 9313–9321, https://doi.org/10.1039/c4ta01783h.
[43] C.L. Yeh, H.C. Hsi, K.C. Li, C.H. Hou, Improved performance in capacitive deionization of activated carbon electrodes with a tunable mesopore and micropore ratio, Desalination 367 (2015) 60–68, https://doi.org/10.1016/j.desal.2015.03.035.
[44] S. Pawlowski, J.G. Crespo, S. Velizarov, Pressure drop in reverse electrodialysis: experimental and modeling studies for stacks with variable number of cell pairs, J Memb Sci 462 (2014) 96–111, https://doi.org/10.1016/j.memsci.2014.03.020.
[45] S. Il Jeon, J.G. Yeo, S. Yang, J. Choi, D.K. Kim, Ion storage and energy recovery of a flow-electrode capacitive deionization process, J Mater Chem A Mater 2 (2014) 6378–6383, https://doi.org/10.1039/c4ta00377b.
[46] S. Yang, J. Choi, J.G. Yeo, S. Il Jeon, H.R. Park, D.K. Kim, Flow-electrode capacitive deionization using an aqueous electrolyte with a high salt concentration, Environ. Sci. Technol. 50 (2016) 5892–5899, https://doi.org/10.1021/acs.est.5b04640.
[47] Y. Cho, K.S. Lee, S.C. Yang, J. Choi, H.R. Park, D.K. Kim, A novel three-dimensional desalination system utilizing honeycomb-shaped lattice structures for flow-electrode capacitive deionization, energy, Environ. Sci. 10 (2017) 1746–1750, https://doi.org/10.1039/c7ee00698e.
[48] H.M. Saif, R.M. Huertas, S. Pawlowski, J.G. Crespo, S. Velizarov, Development of highly selective composite polymeric membranes for Li+/Mg2+ separation, J Memb Sci 620 (2021), https://doi.org/10.1016/j.memsci.2020.118891.
[49] K. Zhang, J. Sun, L. E, C. Ma, S. Luo, Z. Wu, W. Li, S. Liu, Effects of the pore structure of commercial activated carbon on the electrochemical performance of supercapacitors, J Energy Storage 45 (2022), https://doi.org/10.1016/j.est.2021.103457.
[50] H. Kwon, D. Kim, D.G. Kim, H. Choi, J.G. Park, J.H. Son, E. Ali, H. Park, S.C. Yang, Design of a flow channel with vortex generators for performance improvement of flow-electrode capacitive mixing under low pressure drop conditions, Desalination 577 (2024), https://doi.org/10.1016/j.desal.2024.117418.
[51] M.D. Stoller, S. Park, Z. Yanwu, J. An, R.S. Ruoff, Graphene-based ultracapacitors, Nano Lett. 8 (2008) 3498–3502, https://doi.org/10.1021/nl802558y.
[52] M. Biswal, A. Banerjee, M. Deo, S. Ogale, From dead leaves to high energy density supercapacitors, Energy, Environ. Sci. 6 (2013) 1249–1259, https://doi.org/10.1039/c3ee22325f.